Faraday Discussions

Cite this: *Faraday Discuss.*, 2019, **214**, 441

PAPER

Unearthing the factors governing site specific rates of electronic excitations in multicomponent plasmonic systems and catalysts†

Steven Chavez, Vishal Govind Rao and Suljo Linic *

Received 2nd October 2018, Accepted 8th November 2018
DOI: 10.1039/c8fd00143j

We use experimental and computational studies of core–shell metal–semiconductor and metal–molecule systems to investigate the mechanism of energy flow and energetic charge carrier generation in multicomponent plasmonic systems. We demonstrate that the rates of plasmon decay through the formation of energetic charge carriers are governed by two factors: (1) the intensity of the local plasmon induced electric fields at a specific location in the multicomponent nanostructure, and (2) the availability of direct, momentum conserved electronic excitations in the material located in that specific location. We propose a unifying physical framework that describes the flow of energy in all multicomponent plasmonic systems and leads us towards molecular control of the energy flow and excited charge carrier generation in these systems.

1. Introduction

Localized surface plasmon resonance (LSPR) is a collective and coherent oscillation of free electrons in plasmonic nanoparticles stimulated by electromagnetic radiation.[1–3] LSPR is accompanied by large optical extinction cross-sections at the resonant frequencies as well as elevated oscillating electric fields at the surface of the nanostructures. Compared to the electric fields of an incoming photon flux, these fields can be enhanced anywhere from 10^3 times at the surface of single particles to 10^6 times in between two particles separated by $\sim$1 nm.[4–7] LSPR essentially acts to confine incoming electromagnetic energy within small nanovolumes at the surface of the nanoparticles. The energy of these enhanced fields is dissipated either radiatively *via* reemission of photons into the far field (scattering) or non-radiatively *via* the excitation of charge carriers (*i.e.* the formation of energetic electron/hole pairs) within the nanoparticle (absorption). In clean nanoparticles, the energy of these charge carriers is thermalized, *i.e.*, it is

Department of Chemical Engineering, University of Michigan – Ann Arbor, Ann Arbor, Michigan, 48109, USA. E-mail: linic@umich.edu

† Electronic supplementary information (ESI) available. See DOI: 10.1039/c8fd00143j

dissipated as heat directly within the nanostructure *via* electron–electron and subsequently electron–phonon collisions. This thermalization process leads to direct heating of the plasmonic nanostructure under LSPR conditions.[8,9]

Due to their high optical extinction cross-section and their ability to localize electric fields in small volumes, plasmonic nanoparticles are emerging as one of the most promising materials platforms for various applications. Many potential applications of plasmonic nanoparticles rely on spatially controlling the electronic excitation processes in plasmonic nanostructures. Specifically, there is a great deal of interest in creating multifunctional nanostructures where plasmonic nanoparticles that serve as nanoscopic light-energy concentrators are coupled with another material (metal, semiconductor or molecular entities) that utilizes this energy to perform a function.[10–17] In these multifunctional materials, energetic charge carriers would need to transfer from the plasmonic material to the other material before they are thermalized in the plasmonic metal, or preferentially form at high rates (stimulated by LSPR) directly in the other material rather than in the plasmonic metal (Fig. 1). For example, the efficient creation of energetic charge carriers in semiconductors or molecules or the efficient transfer of energetic charge carriers from plasmonic nanoparticles to the attached semiconductors or molecules is crucial in numerous applications including plasmon-enhanced photovoltaics,[18,19] plasmonic sensing,[20] plasmonic photocatalysis[21–25] and photothermal cancer therapy.[26–29] To be able to design such multifunctional nanostructures, a deeper understanding of the energy dissipation pathways in resonantly excited plasmonic multicomponent nanostructures and the factors that govern the flow of energy within these multicomponent plasmonic nanostructures is required.

We have previously reported the design of bimetallic plasmonic nanostructures in the form of Ag–Pt core–shell nanocubes in which relatively large Ag cubes (tens of nanometers) were covered with very thin Pt shells (~1 nm).[30] We demonstrated that in these multimetallic nanostructures, the plasmonic Ag core

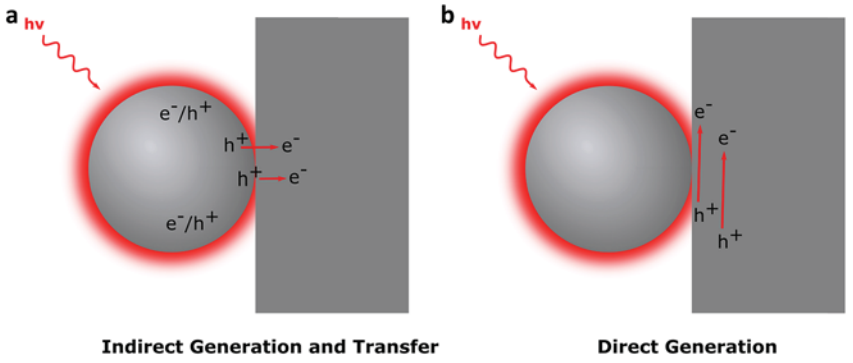

Fig. 1 Mechanisms of energetic charge generation/extraction from plasmonic nanoparticles to surrounding materials. (a) The electron–hole pairs are generated directly in the plasmonic nanostructure. A number of charge carriers with enough energy have an opportunity to transfer over to an attached material. The rest will be thermalized within the bulk of the plasmonic nanostructure. (b) The electron–hole pairs are generated directly in the attached material in regions close to the plasmonic nanostructure. This bypasses thermalization processes in the plasmonic nanostructure.

served to harvest the light energy through the excitation of LSPR and that this LSPR energy was dissipated preferentially through the formation of energetic charge carriers in the thin non-plasmonic Pt shell. We also developed a transparent physical framework that could describe the energy flow in this bimetallic plasmonic system.[31] We postulated that the local rate of formation of energetic charge carriers in the multimetallic nanostructures is to a large degree governed by two factors: (1) the local intensity of the electric field, and (2) the magnitude of the imaginary part of the dielectric function (ε_2) of the non-plasmonic metal relative to the plasmonic metal. In the above-mentioned Ag–Pt core–shell system, the Ag core confined the high field to the surface due to the plasmonic effect, and Pt has a significantly higher ε_2 than Ag at the LSPR frequencies (due to the availability of direct d to s electronic excitations). This led to the dissipation of LSPR energy through the formation of energetic e–h pairs directly in thin Pt shell. This proposed model and the experimental results provided us with a framework for the rational design of multicomponent systems where a plasmonic material guides the light energy to specific, sub-diffraction-limit volumes where this energy is dissipated through the formation of energetic charge carriers at high rates.

To further validate the proposed model for the flow of LSPR energy in multicomponent plasmonic systems, we move away from the above-mentioned bimetallic systems and focus on multicomponent metal–semiconductor and metal–molecule systems. We use experimental and theoretical studies to systematically investigate the LSPR decay mechanisms in core–shell Ag–Cu_2O (metal–semiconductor) and Ag–Methylene Blue (MB) (metal–molecule) multicomponent nanostructures. We show that the high fields generated at the LSPR wavelength can direct energy into the thin Cu_2O and MB shells, respectively, in a manner similar to the one described for the Ag–Pt core–shell structures. This results in the increased absorption in Cu_2O and the MB dye molecules, respectively.

2. Metal–semiconductor systems

To synthesize the Ag–Cu_2O core–shell nanostructures, we first synthesized Ag nanocube seeds using a well-established polyol-based method.[32–34] The resulting nanocubes were characterized using high-angle annular dark field scanning transmission electron microscopy (STEM). The average edge length of the Ag nanocubes was determined to be ~75 nm. The Ag nanocube seeds were then coated with a thin layer of Cu_2O by modifying a recently reported method.[35] Briefly, the Ag–Cu_2O nanoparticles were prepared by reducing a copper(II) nitrate precursor onto the Ag nanocube seeds with hydrazine in the presence of sodium hydroxide and polyvinylpyrrolidone. This resulted in the conformal coating of Cu_2O onto the surface of the Ag nanocubes. Fig. 2a shows a representative bright field STEM image of the Ag–Cu_2O nanocubes investigated in this study. Elemental mapping of the particles (Fig. 2b–e) using energy dispersive X-ray spectroscopy (EDS) shows that the Ag nanocube cores are covered by the Cu_2O shells. From the STEM images, we determined the average thickness of the Cu_2O shell to be ~5 nm.

To investigate the impact of the thin Cu_2O shell on the energy flow in these core–shell nanostructures, we studied the optical properties of the Ag–Cu_2O nanostructures by measuring their extinction, absorption and scattering and comparing these to the optical properties of the pure Ag nanocube seeds of

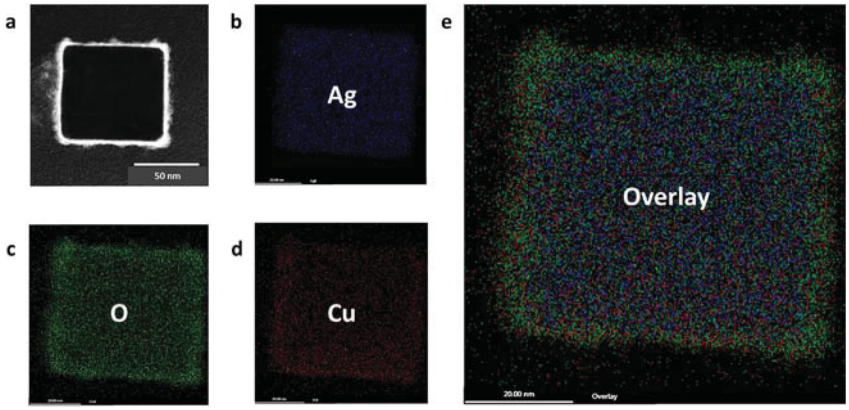

Fig. 2 (a) Bright field STEM image of a representative Ag–Cu_2O nanocube. The average edge length of the nanocubes was ~75 ± 2 nm. EDS elemental maps of Ag (b), O (c), Cu (d) and their overlay (e).

comparable size. The extinction characteristics of the nanocubes were measured using transmission UV-vis spectroscopy. The UV-vis data in Fig. 3a show that the introduction of the thin Cu_2O shell results in a slight red-shift and an increased linewidth of the LSPR extinction peak. This red-shift in the LSPR peak is the result of the higher refractive index of Cu_2O compared to air.[36] Additionally, the extinction linewidth is related to the plasmon lifetime, where larger linewidths correspond to shorter plasmon lifetimes.[37] Furthermore, an optical integrating

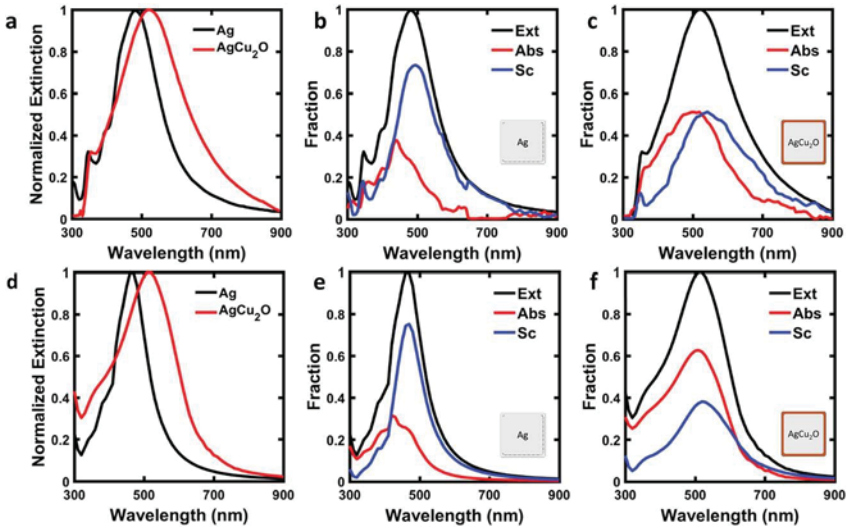

Fig. 3 (a) Measured normalized extinction of the Ag and Ag–Cu_2O nanocubes; (b and c) measured fractional extinction, absorption and scattering of (b) the Ag nanocubes, and (c) the Ag–Cu_2O nanocubes; (d) calculated normalized extinction of the Ag and Ag–Cu_2O nanocubes; (e and f) calculated fractional extinction, absorption and scattering of (e) the Ag nanocubes, and (f) the Ag–Cu_2O nanocubes. The edge dimensions of the Ag cube in the calculations was 75 nm and the thickness of the Cu_2O shell was 5 nm.

sphere was used to measure the partitioning between absorption and scattering for the Ag–Cu_2O nanocubes as well as the pure Ag nanocubes. The data in Fig. 3b and c show that the introduction of the Cu_2O shell modifies the LSPR decay pathway, resulting in an increased ratio of absorption to scattering when compared to the pure Ag nanocubes. Based on these data, we hypothesized that: (1) the Cu_2O shell was providing a faster pathway for the dissipation of the electromagnetic energy than Ag, and that the energy was preferentially dissipated through the absorption process in the thin Cu_2O shell. In other words, the introduction of Cu_2O at the surface increased the rate of formation of energetic e–h pairs at the surface of the nanostructure compared to the case of pure Ag; and (2) the presence of the Ag core increases the absorption rates (the rate of formation of charge carriers) in the Cu_2O shell, compared to the identical Cu_2O shell without the Ag plasmonic core effect.

Since the experimental data in Fig. 3 does not inform us about the location of the energetic e–h pair formation under the LSPR conditions, we performed finite element method (FEM) electrodynamic simulations to spatially resolve the absorption process within the nanostructures. The geometry constructed for the FEM model consisted of a 75 nm Ag nanocube surrounded by a 5 nm shell (corresponding to the dimensions determined from the STEM images) and the dielectric properties for Ag and Cu_2O were obtained from standard databases.[38,39] The data in Fig. 3d–f show that the calculated extinction, absorption and scattering properties for the Ag and Ag–Cu_2O core–shell nanocubes are consistent with the experimental measurements, showing that scattering is the dominant plasmon decay pathway for pure Ag cubes while absorption dominates for the Ag–Cu_2O particles.

We used the FEM model to shed light on the two hypotheses, (1) and (2) discussed above, that emerged from our experimental measurement of the optical properties. The data in Fig. 4a show the calculated power dissipated as a function of wavelength in the Cu_2O shell for the Ag–Cu_2O particle compared to the

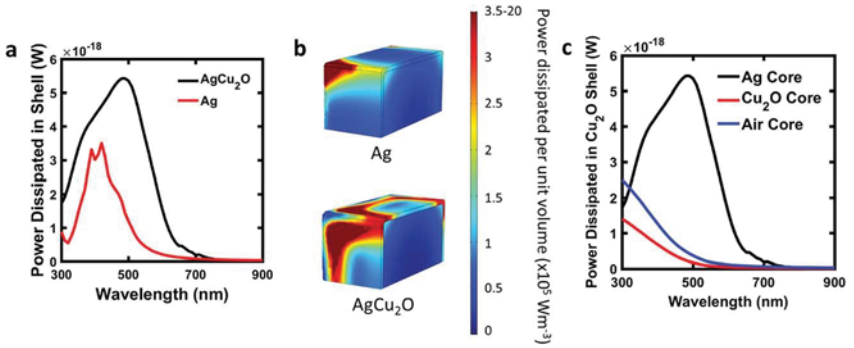

Fig. 4 (a) Total power dissipated as a function of wavelength in the particle shells for the Ag–Cu_2O particle and the Ag–Ag core–shell particle; (b) contour maps of the power dissipation per unit volume at the LSPR frequencies for the pure Ag particle and the Ag–Cu_2O particle. Due to the symmetry of the structures, we show the maps for a quarter of the cubes; (c) total power dissipated in the Cu_2O shell of core–shell particles with varying core materials. The source field for all simulations was 1 V m^{-1} at all frequencies, which for a free space amounts to 2.6×10^{-4} mW cm^{-2}.

calculated energy dissipation rate in a virtual Ag 'shell' of a reference Ag–Ag core–shell nanocube of identical dimensions. The calculated power is essentially a measure of the wavelength-dependent rate of formation of energetic e–h pairs in the shell. The data in Fig. 4a show that, as was hypothesized, the introduction of the thin Cu_2O shell increased the rate of formation of energetic e–h pairs at the surface of the nanostructure (in the thin Cu_2O shell region) compared to the case of pure Ag, *i.e.*, the process of photon absorption is shifted to the surface layers of the multicomponent nanostructure. This is further shown in Fig. 4b, which shows simulated contour maps of the power dissipated throughout the pure Ag nanocube compared to the Ag–Cu_2O nanocube. Upon integrating the power dissipated throughout the shells in these systems (*i.e.* the data in Fig. 4a) with respect to energy, we determined that ~6 times as much energy was being deposited through the shell of the Ag–Cu_2O particle than in the Ag shell of the pure Ag particle of identical size. To test the second hypothesis, we calculated the rate of absorption in the Cu_2O shell of the Ag–Cu_2O nanoparticle and compared it to the absorption of a Cu_2O shell with identical dimensions, supported on either a pure Cu_2O core or in the absence of a core (*i.e.* the core was defined as air). The data in Fig. 4c show that the absorption (*i.e.* generation of charge carriers) in the semiconductor (Cu_2O) shell, at the LSPR wavelengths, is significantly larger for the particle with the Ag plasmonic core. This suggests that in systems where a thin semiconductor shell is surrounding a plasmonic nanoparticle core, the plasmonic core can serve to enhance the rates of absorption in the shell compared to when the shell is supported on non-plasmonic materials.

As discussed above, we postulated that the site-specific rate of formation of energetic charge carriers in the multicomponent plasmonic nanostructures is to a large degree governed by two factors: (1) the intensity of the LSPR-induced electric field at the specific site, and (2) the magnitude of ε_2 of the material that resides at the site. We used the data in Fig. 3 and 4 to test the validity of the model. The first question is related to the impact of the local E-field on the rate of energy dissipation *via* absorption (*i.e.*, the rate of LSPR decay *via* localized absorption). It is well established that plasmonic nanostructures generate high electric fields that are confined to the surface of the nanostructure.[5,40] To investigate how the LSPR decay is affected by the field enhancement, we used the FEM model to calculate the electric field intensity $|E|^2$ as a function of wavelength at the surface of the Ag nanoparticle (specifically, at the Ag–Cu_2O interface) with the Cu_2O shell (Fig. 5a). Comparing these wavelength-dependent E-field intensities with the wavelength-dependent rate of absorption in the surface-bound thin Cu_2O shell (Fig. 4c) shows that the wavelength-dependent rate of absorption in the Cu_2O shell is heavily influenced by the magnitude of the electric field, where larger wavelength-dependent fields induce higher absorption rates. Furthermore, we have also divided the rate of absorption in the Cu_2O shell of the Ag–Cu_2O core–shell nanoparticle by the rate of absorption in the Cu_2O shell with identical dimensions, supported on either a pure Cu_2O core or on an air-filled core (as described above), and compared these ratios to ratios in the E-field intensity of the respective systems. The data in Fig. 5b show there is a quantitative agreement between the ratios in the local field intensities and the ratios in the local rates of absorption in the Cu_2O shells. This analysis shows that for a given multicomponent plasmonic material, it is the electric field induced by the plasmonic component that drives the process of photon absorption, *i.e.*, a higher local field

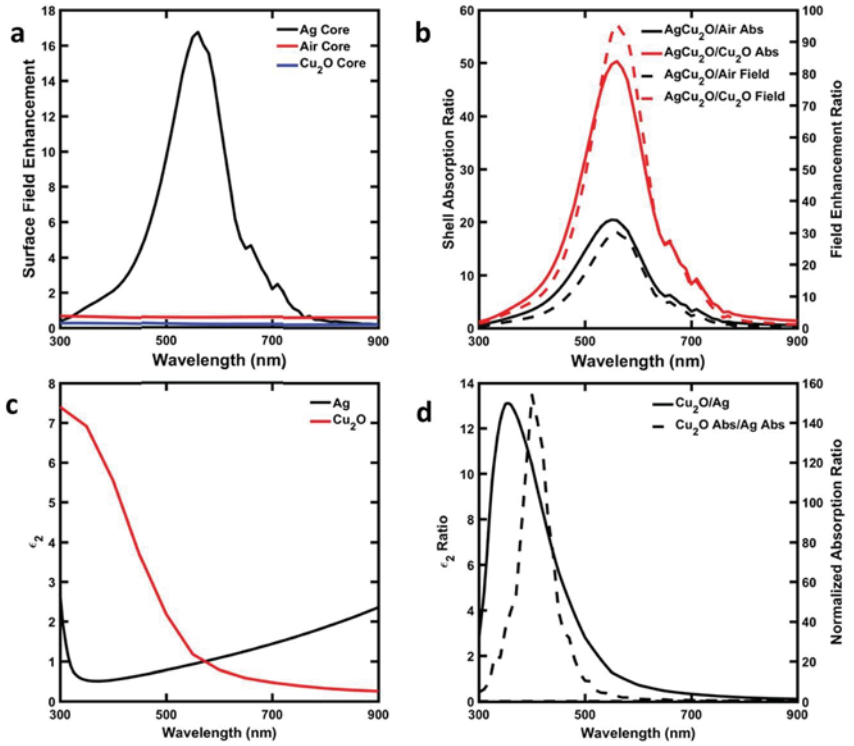

Fig. 5 (a) Calculated electric field enhancements at the core-Cu_2O interface for the varying core materials (Ag, air or Cu_2O); (b) field enhancement ratios (dashed lines) and shell absorption ratios (solid lines) for Ag–Cu_2O with respect to both the Cu_2O–Cu_2O and the Cu_2O–air core–shell systems; (c) the imaginary part of the dielectric function (ε_2) for both Ag and Cu_2O; (d) the ratio of ε_2 of Cu_2O and Ag (solid line) and the E-field-normalized shell absorption ratios of Cu_2O in the Ag–Cu_2O system and Ag in the Ag–Ag system (dashed line).

will induce higher rates of absorption. For a given material (in this case Cu_2O), these local plasmonic E-fields can significantly increase the rates of absorption compared to the situations where these fields are not present.

The second issue we address is related to the impact of the local imaginary part of the dielectric function (ε_2) on the energy dissipation pathway in multicomponent plasmonic nanostructures. The data in Fig. 4a show that the rate of energy dissipation is higher in the Cu_2O shell of the Ag–Cu_2O core–shell nanoparticle than in the Ag shell of the virtual Ag–Ag core–shell structure over a wide range of wavelengths. To explain this result, we plotted the value of ε_2 as a function of wavelength for Cu_2O and Ag in Fig. 5c. The data show that ε_2 is larger for Cu_2O than for Ag at wavelengths below ~590 nm, *i.e.*, at the wavelengths where the LSPR is excited. This difference in the value of ε_2 of the shell material can qualitatively explain the higher rate of energy dissipation through the Cu_2O shell compared to the virtual Ag shell. We note that this discrepancy in the magnitudes of ε_2 for Ag and Cu_2O stems from the difference in electronic structure. The magnitude of ε_2 of a material is directly related to the availability of direct momentum conserving electronic transitions in the material. Since Ag is a d^{10}

metal, its d band lies low in energy and direct, momentum conserved transitions are improbable at low photon energies, resulting in a low value of ε_2 in the visible range.[22] Above 2.1 eV, Cu_2O has a direct band gap, meaning its electronic transitions are momentum-conserved and it can efficiently absorb UV-visible photons with energy higher than 2.1 eV, resulting in a high ε_2 above this threshold energy.

Comparing these values of ε_2 for Cu_2O and Ag (Fig. 5c) with the rate of absorption in the Cu_2O shell in the Ag–Cu_2O particle and the equivalent Ag shell of a pure Ag nanoparticle (Fig. 4a) suggests that the availability of these direct electronic excitations in Cu_2O (that lead to high ε_2) is responsible for the elevated rates of plasmon decay in the Cu_2O shell. We note that the plasmonic E-field is different for the virtual Ag shell of the pure Ag nanocube compared to the Ag–Cu_2O nanocube. This difference in the E-field leads to some deviation in the agreement between the rate of energy dissipation through the Ag and Cu_2O shells and the relative magnitudes of ε_2 of the shell material. To account for this difference in the E-field we have normalized the shell absorption ratio in the Cu_2O and Ag shells on the Ag–Cu_2O and Ag–Ag nanostructures with the ratio of their respective E-field intensities. The data in Fig. 5d shows that the quantity that we obtain this way scales very well with the ratio of ε_2 for Cu_2O and Ag. This essentially means that for the systems where the local E-field is similar, the rate of energy dissipation *via* absorption can be nicely approximated by the value of ε_2. Simply put, by positioning a material with a larger ε_2 (compared to the plasmonic material) on the surface of a plasmonic nanostructure, the absorption channel is preferentially directed to that material.

3. Metal–molecule systems

The analysis presented above describes that the ability of plasmonic nanostructures to guide and dissipate energy in particular locations of a multicomponent plasmonic nanosystem is governed by two critical factors: (i) the local intensity of the electric field, and (ii) the availability of direct electronic transitions (high ε_2) at the wavelengths where the electric fields are high. To further generalize this model, we experimentally and computationally analyzed the optical properties of 75 nm Ag nanocubes interacting with methylene blue (MB) dye molecules. We created our Ag–MB solution by mixing a solution of ~75 nm Ag nanocubes dispersed in water with MB dye molecules. The resulting concentration of the MB in solution was 340 nM. It has been shown that at these low concentrations, the Ag particles are essentially surrounded by thin layers of MB, *i.e.*, solid state MB is adsorbed on the surface of Ag nanoparticles.[41] We used an integrating sphere to measure the optical characteristics (*i.e.* extinction, absorption and scattering) of our Ag–MB samples and compared them to the optical properties of a pure Ag nanocube solution of the same Ag cube concentration. The optical data in Fig. 6a and b show that the introduction of MB into the solution increases the overall absorption in the region around ~665 nm. MB is a dye molecule characterized by strong absorption at ~665 nm. To determine the effect of the Ag nanocubes on the MB absorption, we calculated the absorption in MB on the Ag nanocube surface by subtracting the pure Ag absorption from the Ag–MB absorption (the MB concentration is 340 nM) and comparing it to the absorption of a pure MB solution (340 nM). The data in Fig. 6c show that at the wavelength

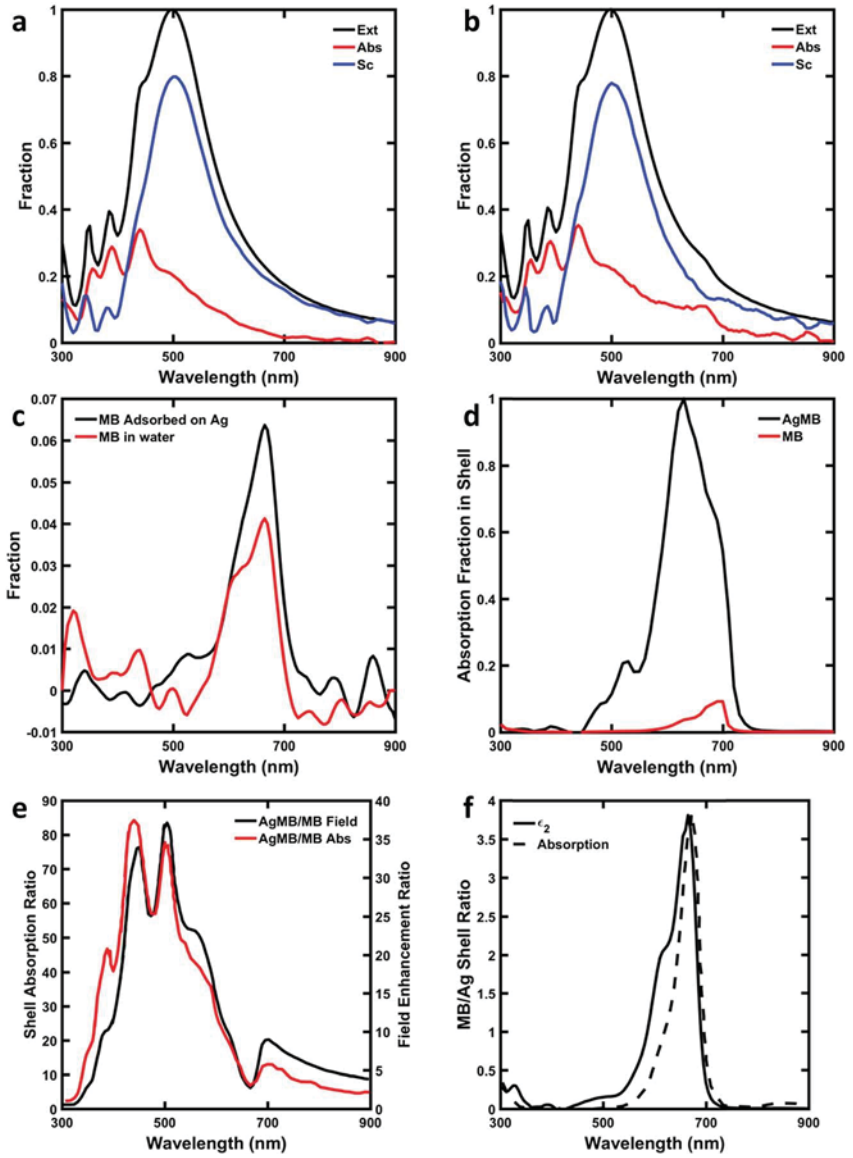

Fig. 6 (a and b) Measured fractional extinction, absorption and scattering of (a) the Ag nanocubes, and (b) the Ag–MB system; (c) absorption of MB in water (red line) and absorption of MB on the Ag nanoparticle surface; (d) calculated absorption in the Ag–MB shell *vs.* the MB shell in a reference MB shell with an MB core system; (e) field enhancement ratios and shell absorption ratios for Ag–MB with respect to the pure MB system; (f) the ratio of ε_2 of MB and Ag *vs.* the field normalized shell absorption ratios of MB in the Ag–MB system and Ag in the Ag–Ag system.

where MB absorbs, the absorption in MB in the presence of the Ag nanocubes is larger than that without the Ag nanocubes.

We used the FEM model to simulate the optical characteristics of these systems. The MB dielectric properties were determined by measuring the

absorption cross section of the 340 nM MB solution (with UV-vis spectroscopy) and applying the Kramers–Kronig relations as shown previously.[42] The model system used in the FEM simulations consisted of a Ag nanocube with an edge length of 75 nm covered with a 1 nm MB "shell". To draw conclusions about the factors that govern the energy flow in these systems, we also modeled the behavior of two control model systems: an Ag–Ag core–shell nanocube (similar to one used above) and an MB–MB core–shell nanocube, both of identical dimensions to the Ag–MB nanocube. The data in Fig. 6d show that the simulated absorption spectra for MB on Ag (*i.e.*, the shell of the Ag–MB core shell model system) qualitatively match the experiments. The discrepancy in the spectral peak shape of the simulated MB absorption for the Ag–MB core–shell system compared to the experimentally measured absorption (Fig. 6c, dark line) stems from the fact that the absorption data in Fig. 6c is for solid MB films attached to Ag while the simulated spectra uses the MB dielectric function derived for low concentration mainly isolated MB molecules. We study the impact of the LSPR E-field on the absorption in this system by calculating the ratio of the absorption of MB in the Ag–MB core–shell system to the absorption in the MB shell of a model MB–MB core–shell system and comparing it to the ratio of field intensity at the respective core–shell interfaces (*i.e.* the ratio of the fields with and without a plasmonic Ag core). The data in Fig. 6e show that, like in the Ag–Cu_2O case, the absorption ratio tracks with the field ratio, demonstrating that the enhanced absorption in the shell is plasmon induced. Additionally, we explored the effect of ε_2 in this system by calculating the ratio of shell absorption in the Ag–MB particle to the shell absorption in the pure Ag particle and correcting it by the respective field contributions (in a similar manner to the Ag–Cu_2O case described above). The obtained data quantitatively track very well the calculated ratio of ε_2 for MB and Ag (Fig. 6f).

Conclusions

In summary, by studying multicomponent (*i.e.* core–shell metal–semiconductor and metal–molecule) systems, we demonstrated that both the electric field intensity under resonant LSPR conditions and the value of ε_2 of the shell relative to the core are the critical factors governing the flow of energy in these systems. In the metal–semiconductor case, we studied core–shell Ag–Cu_2O nanocubes. We showed that the presence of the Cu_2O shell altered the LSPR decay pathway, resulting in high absorption directly in the Cu_2O shell. We showed that this enhanced absorption process was field driven and that the field energy was dissipated to a greater extent when the shell material had a higher ε_2 with respect to the core material. Additionally, we showed that this framework also described the flow of energy in metal–molecule systems for the case of MB adsorbed on Ag nanocubes.

Conflicts of interest

There are no conflicts of interest to declare.

Acknowledgements

The work presented in this document was supported by the National Science Foundation (NSF) (CHE-1800197). Secondary support was provided by the

National Science Foundation (NSF) (CHE-17024711) (analysis of molecular interactions with nanostructures) and the Office of Basic Energy Science, Division of Chemical Sciences (FG-02-05ER15686) (materials synthesis). S. L. also acknowledges the partial support of the Technische Universität München – Institute for Advanced Study, funded by the German Excellence Initiative and the European Union Seventh Framework Programme under grant agreement no. 291763.

References

1 M. A. El-Sayed, Some Interesting Properties of Metals Confined in Time and Nanometer Space of Different Shapes, *Acc. Chem. Res.*, 2001, **34**, 257–264.
2 K. L. Kelly, E. Coronado, L. L. Zhao and G. C. Schatz, The Optical Properties of Metal Nanoparticles: The Influence of Size, Shape, and Dielectric Environment, *J. Phys. Chem. B*, 2003, **107**, 668–677.
3 C. F. Bohren and D. R. Huffman, *Absorption and Scattering of Light by Small Particles*, Wiley, 1998, p. 544.
4 L. Gunnarsson, T. Rindzevicius, J. Prikulis, B. Kasemo, M. Käll, S. Zou and G. C. Schatz, Confined Plasmons in Nanofabricated Single Silver Particle Pairs: Experimental Observations of Strong Interparticle Interactions, *J Phys. Chem. B*, 2004, **109**, 1079–1087.
5 E. Hao and G. C. Schatz, Electromagnetic Fields around Silver Nanoparticles and Dimers, *J. Chem. Phys.*, 2004, **120**, 357.
6 J. Jiang, K. Bosnick, M. Maillard and L. Brus, Single Molecule Raman Spectroscopy at the Junctions of Large Ag Nanocrystals, *J. Phys. Chem. B*, 2003, **107**, 9964–9972.
7 S. Linic, P. Christopher and D. B. Ingram, Plasmonic-Metal Nanostructures for Efficient Conversion of Solar to Chemical Energy, *Nat. Mater.*, 2011, **10**, 911–921.
8 C. Frischkorn and M. Wolf, Femtochemistry at Metal Surfaces: Nonadiabatic Reaction Dynamics, *Chem. Rev.*, 2006, **106**, 4207–4233.
9 M. L. Brongersma, N. J. Halas and P. Nordlander, Plasmon-Induced Hot Carrier Science and Technology, *Nat. Nano.*, 2015, **10**, 25–34.
10 A. M. Brown, R. Sundararaman, P. Narang, W. A. Goddard and H. A. Atwater, Nonradiative Plasmon Decay and Hot Carrier Dynamics: Effects of Phonons, Surfaces, and Geometry, *ACS Nano*, 2016, **10**, 957–966.
11 K. Li, N. J. Hogan, M. J. Kale, N. J. Halas, P. Nordlander and P. Christopher, Balancing Near-Field Enhancement, Absorption, and Scattering for Effective Antenna–Reactor Plasmonic Photocatalysis, *Nano Lett.*, 2017, **17**, 3710–3719.
12 M. Bernardi, J. Mustafa, J. B. Neaton, S. G. Louie, W. L. Barnes, A. Dereux, T. W. Ebbesen, M. Tame, J. S. Fakonas, H. Lee, *et al.*, Theory and Computation of Hot Carriers Generated by Surface Plasmon Polaritons in Noble Metals, *Nat. Commun.*, 2015, **6**, 7044.
13 A. Joplin, S. Ali Hosseini Jebeli, E. Sung, N. Diemler, P. J. Straney, M. Yorulmaz, W.-S. Chang, J. E. Millstone and S. Link, Correlated Absorption and Scattering Spectroscopy of Individual Platinum-Decorated Gold Nanorods Reveals Strong Excitation Enhancement in the Nonplasmonic Metal, *ACS Nano*, 2017, **11**, 12346–12357.

14 S. Linic, U. Aslam, C. Boerigter and M. Morabito, Photochemical Transformations on Plasmonic Metal Nanoparticles, *Nat. Mater.*, 2015, **14**, 567–576.
15 K. Wu, J. Chen, J. R. McBride, T. Lian, H. A. Atwater, A. Polman, C. Clavero, S. Linic, P. Christopher, D. B. Ingram, *et al.*, CHARGE TRANSFER. Efficient Hot-Electron Transfer by a Plasmon-Induced Interfacial Charge-Transfer Transition, *Science*, 2015, **349**, 632–635.
16 C. Boerigter, U. Aslam and S. Linic, Mechanism of Charge Transfer from Plasmonic Nanostructures to Chemically Attached Materials, *ACS Nano*, 2016, **10**, 6108–6115.
17 C. Boerigter, R. Campana, M. Morabito and S. Linic, Evidence and Implications of Direct Charge Excitation as the Dominant Mechanism in Plasmon-Mediated Photocatalysis, *Nat. Commun.*, 2016, **7**, 10545.
18 H. a. Atwater and A. Polman, Plasmonics for Improved Photovoltaic Devices, *Nat. Mater.*, 2010, **9**, 205–213.
19 F. J. Beck, A. Polman and K. R. Catchpole, Tunable Light Trapping for Solar Cells Using Localized Surface Plasmons, *J. Appl. Phys.*, 2009, **105**, 114310.
20 M. W. Knight, H. Sobhani, P. Nordlander and N. J. Halas, Photodetection with Active Optical Antennas, *Science*, 2011, 332.
21 P. Christopher, H. Xin and S. Linic, Visible-Light-Enhanced Catalytic Oxidation Reactions on Plasmonic Silver Nanostructures, *Nat. Chem.*, 2011, **3**, 467.
22 U. Aslam, V. G. Rao, S. Chavez and S. Linic, Catalytic Conversion of Solar to Chemical Energy on Plasmonic Metal Nanostructures, *Nat. Catal.*, 2018, **1**, 656–665.
23 S. Mukherjee, F. Libisch, N. Large, O. Neumann, L. V. Brown, J. Cheng, J. B. Lassiter, E. A. Carter, P. Nordlander and N. J. Halas, Hot Electrons Do the Impossible: Plasmon-Induced Dissociation of H_2 on Au, *Nano Lett*, 2013, **13**, 240–247.
24 S. Mubeen, J. Lee, N. Singh, S. Krämer, G. D. Stucky and M. Moskovits, An Autonomous Photosynthetic Device in Which All Charge Carriers Derive from Surface Plasmons, *Nat. Nano.*, 2013, **8**, 247–251.
25 P. Christopher, H. Xin, A. Marimuthu and S. Linic, Singular Characteristics and Unique Chemical Bond Activation Mechanisms of Photocatalytic Reactions on Plasmonic Nanostructures, *Nat. Mater.*, 2012, **11**, 1044.
26 X. Huang, I. H. El-Sayed, W. Qian and M. A. El-Sayed, Cancer Cell Imaging and Photothermal Therapy in the Near-Infrared Region by Using Gold Nanorods, *JACS*, 2006, **128**, 2115–2120.
27 L. B. Carpin, L. R. Bickford, G. Agollah, T.-K. Yu, R. Schiff, Y. Li and R. A. Drezek, Immunoconjugated Gold Nanoshell-Mediated Photothermal Ablation of Trastuzumab-Resistant Breast Cancer Cells, *Breast Cancer Res. Treat.*, 2011, **125**, 27–34.
28 M. R. K. Ali, Y. Wu, Y. Tang, H. Xiao, K. Chen, T. Han, N. Fang, R. Wu and M. A. El-Sayed, Targeting Cancer Cell Integrins Using Gold Nanorods in Photothermal Therapy Inhibits Migration through Affecting Cytoskeletal Proteins, *Proc. Natl. Acad. Sci. U. S. A.*, 2017, **114**, E5655–E5663.
29 I. H. El-Sayed, X. Huang and M. A. El-Sayed, Selective Laser Photo-Thermal Therapy of Epithelial Carcinoma Using Anti-EGFR Antibody Conjugated Gold Nanoparticles, *Cancer Lett.*, 2006, **239**, 129–135.

30 U. Aslam, S. Chavez and S. Linic, Controlling Energy Flow in Multimetallic Nanostructures for Plasmonic Catalysis, *Nat. Nano.*, 2017, **12**, 1000–1005.
31 S. Chavez, U. Aslam and S. Linic, Design Principles for Directing Energy and Energetic Charge Flow in Multicomponent Plasmonic Nanostructures, *ACS Energy Lett.*, 2018, **3**, 1590–1596.
32 Y. Sun and Y. Xia, Shape-Controlled Synthesis of Gold and Silver Nanoparticles, *Science*, 2002, **298**, 2176–2179.
33 S. Linic and P. Christopher, Overcoming Limitation in the Design of Selective Solid Catalysts by Manipulating Shape and Size of Catalytic Particles: Epoxidation Reactions on Silver, *ChemCatChem*, 2010, **2**, 1061–1063.
34 T. Van Cleve, E. Gibara and S. Linic, Electrochemical Oxygen Reduction Reaction on Ag Nanoparticles of Different Shapes, *ChemCatChem*, 2016, **8**, 256–261.
35 H. Jing, N. Large, Q. Zhang and H. Wang, Epitaxial Growth of Cu_2O on Ag Allows for Fine Control Over Particle Geometries and Optical Properties of Ag–Cu_2O Core–Shell Nanoparticles, *J Phys. Chem. C.*, 2014, **118**, 19948–19963.
36 U. Kreibig and M. Vollmer, *Optical Properties of Metal Clusters*, 1995.
37 S. A. Maier, *Plasmonics: Fundamentals and Applications*, Springer, 2007.
38 A. D. Rakić, A. B. Djurišić, J. M. Elazar and M. L. Majewski, Optical Properties of Metallic Films for Vertical-Cavity Optoelectronic Devices, *Appl. Opt.*, 1998, **37**, 5271–5283.
39 C. G. Ribbing and A. Roos, *Handbook of Optical Constants of Solids*, 1997, pp. 875–882.
40 P. L. Stiles, J. A. Dieringer, N. C. Shah and R. P. Van Duyne, Surface-Enhanced Raman Spectroscopy SERS: Surface-Enhanced Raman Spectroscopy Raman Scattering: Inelastic Scattering of a Photon from a Molecule in Which the Frequency Change Precisely Matches the Difference in Vibrational Energy Levels, *Annu. Rev. Anal. Chem*, 2008, **1**, 601–626.
41 B. L. Darby, B. Auguié, M. Meyer, A. E. Pantoja and E. C. Le Ru, Modified Optical Absorption of Molecules on Metallic Nanoparticles at Sub-Monolayer Coverage, *Nat. Photon.*, 2016, **10**, 40–45.
42 A. Djorovic, M. Meyer, B. L. Darby and E. C. Le Ru, Accurate Modeling of the Polarizability of Dyes for Electromagnetic Calculations, *ACS Omega*, 2017, **2**, 1804–1811.